An Analytical calibration approach for the polarimetric Airborne C band Radiometer

Hanh Pham, Edward.J Kim, *Member, IEEE,*

***Abstract*— Passive microwave remote sensing is sensitive to the quantity and distribution of water in soil and vegetation. During summer 2000, the Microwave Geophysics Group at the University of Michigan conducted the seventh Radiobrighness Energy Balance Experiment (REBEX-7) over a corn canopy in Michigan. Long time series of brightness temperatures, soil moisture and micrometeorology on the plot scale were taken. This paper addresses the calibration of the NASA GSFC polarimetric airborne C band microwave radiometer (ACMR) that participated in REBEX-7. These passive polarimeters are typically calibrated using an end-to-end approach based upon a standard artificial target or a well-known geophysical target. Analyzing the major internal functional subsystems offers a different perspective. The primary goal of this approach is to provide a transfer function that not only describes the system in its entirety but also accounts for the contributions of each subsystem toward the final modified Stokes parameters. This approach does not assume that the radiometric system is linear as it does not take polarization isolation for granted, and it also serves as a realistic instrument simulator, a useful tool for future designs. The ACMR architecture can be partitioned into functional subsystems. The characteristics of each subsystem was extensively measured and the estimated parameters were imported into the overall closed form system model. Inversion of the model yields a calibration for the modified Stokes parameters with uncertainties of 0.2 K for the V and H polarizations and 2.4 K for the 3rd and 4th parameters. Application to the full Stokes parameters over a senescent cornfield is presented.**

***Index Terms*— calibration, microwave radiometry, polarimetry.**

I. Introduction

KNOWLEDGE of the state of soil moisture is crucial for near term climate prediction [1]. Passive microwave remote sensing provides a cost effective, all weather tool for observing land surface soil moisture globally at a useful spatial resolution over regions with low to moderate levels of vegetation cover [2]. The influence of absorption and scattering due to vegetation on the microwave signature of soil moisture decreases as lower frequencies are used [3]. The threshold canopy moisture column density ranges between 0.5 and $1.5kg/m^2$ at 19GHz, which makes the Special Sensor Microwave/Imager (SSMI) not practical for determining soil moisture content, and $4kg/m^2$ for L band (1.4 GHz) [4]. Although L band is potentially the most effective frequency for mapping surface soil moisture on a global scale, there are no L band satellite radiometers currently on orbit. The lowest frequency satellite radiometers in orbit are the Advanced Microwave Scanning Radiometer (AMSR-E) with C band (6.9GHz) vertical and horizontal channels, and Windsat with C band (6.6GHz) full Stokes capability. Therefore, for surface soil moisture monitoring from space, C band observations are of interest. Conventional radiometers measure the vertical and horizontal polarized energy of the incident electromagnetic wave. Recently, radiometers with additional polarization capabilities (polarimeters) have been deployed on satellites (Windsat), aircraft (AESMIR, PSR, APMIR) and ground-based platforms (ACMR, TMRS3). It has been demonstrated that polarimetric signatures can be generated by anisotropic surfaces [5]. And, using such full-Stokes instruments, a full description of the radiation field can be obtained and new geophysical retrievals may be explored— for example, the polarimetric retrieval of ocean vector winds [6]. C band observations containing polarimetric measurements over land may provide information on the texture and composition of the targets, as polarimetric signatures due to the anisotropy of tilled row structures of soil have been predicted theoretically [5] and the third Stokes parameter has been measured over a periodic soil surface at X band [7]. Because of the potential scientific relevance of polarimetric signatures for Earth remote sensing, the calibration of radiometers measuring the four modified Stokes parameters, defined under the Raleigh-Jeans approximation as:

$$\begin{pmatrix} T_v \\ T_h \\ T_3 \\ T_4 \end{pmatrix} = \begin{pmatrix} T_v \\ T_h \\ T_{+45^\circ} - T_{-45^\circ} \\ T_{lc} - T_{rc} \end{pmatrix} = \frac{\lambda^2}{\eta k_B} \begin{pmatrix} \langle |E_v|^2 \rangle \\ \langle |E_h|^2 \rangle \\ 2\Re e\langle E_v E_h^\star \rangle \\ 2\Im m\langle E_v E_h^\star \rangle \end{pmatrix} \quad (1)$$

deserves attention. T_v and T_v are respectively, the vertical and horizontal brightness temperatures, in Kelvins. T_{+45° and T_{-45° are respectively, the orthogonal linearly polarized measurements skewed 45°, -45° with respect to normal, in Kelvins, T_{lc} and $-T_{rc}$ are respectively the left hand and right hand circular polarized brightness, in Kelvins. E_v and E_h are respectively, the complex vertical and horizontal field amplitudes for a narrow band of frequencies about f. The brackets $\langle ... \rangle$ denote a time-average process. And η, λ, and k_B are the wave impedance, the wavelength and Boltzmann's constant, respectively.

There are basically two types of polarimeter architectures: polarization combining radiometers and direct correlating. Polarization combining radiometers measure combinations of

Manuscript received July 1, 2004; revised XX x, 2004. This work has been partially sponsored by the GEST Graduate Student Summer Program 2003.

H. Pham is with the Microwave Geophysics Group, at the University of Michigan, Ann Arbor, MI 48109-2143 USA (email:hpham@umich.edu).

E. J. Kim is with the microwave sensors branch, at NASA Goddard Space Flight Center, Greenbelt, MD 21192 USA (email:Edward.J.Kim@nasa.gov).

the above polarizations to synthesize the four Stokes parameters, whereas direct correlating radiometers compute the third and fourth Stokes parameters using analog or digital cross correlation circuitry. The calibration of the vertical and horizontal polarizations is fairly straightforward for total power radiometers [8]. Evaluation of the third and fourth Stokes parameters is more delicate for several reasons:

- Their expected amplitudes can be one to two order of magnitudes smaller than those of the vertical and horizontal polarized signals–e.g., a few Kelvins for ocean vector winds [6],
- due to the practical architectures used, contaminated polarimetric outputs are to be expected. Contamination can stem from cross talk between channels, system leakages, channel unbalances, non-idealities, and receivers instabilities. This is especially true for radiometers based on polarization combining networks or on coherent adding techniques [9].

In order to obtain the third and fourth Stokes parameters with the highest absolute accuracy, several approaches have been adopted. They can be classified into roughly three categories: the development of external polarimetric calibration devices, geophysical model-based calibration, and analytical methods.

The first two calibration approaches consider the polarimeter as a single unit via an end-to-end calibration. The first category strives at designing calibration standards regardless of the polarimeter's configuration: such standards [11] have the advantage of being able to calibrate nearly any polarimeter as long as a perfect mechanical setup is achieved. In the second category, geophysical models support the calibration process [10]; one obvious limitation is the robustness and reliability of the models. These two approaches are attractive as end-to-end calibration techniques. However, they do not necessarily provide any precise design feedback on the instrument's configuration, which can be extremely valuable in designing future instruments. In the third category, radiometer parameters are measured in the laboratory and an instrument simulator based on real performance can be created, and no assumption on the instrument linearity is needed. This approach can give engineering feedback on the instrument design, however, it can suffer from errors associated to laboratory measurements. We note that correlated noise calibration standards [12], [13] are an intermediate calibration tool for polarimeters and can be made flexible enough [15] to help in semi-end-to-end calibration (the antenna being not included) or to inject noise at each successive stage of the instrument. Still, in this latter case, the output of each stage needs to be known, which is similar to the analytical method.

Our objective is to apply the analytical or blockwise method to calibrate ACMR to deliver accurate modified Stokes parameters. This paper is arranged in the following manner. In Section II, we describe the forward model used to account for ACMR subsystem characteristics. Section III describes the experimental characterization of the system blocks, particularly the antenna measurements for passive polarimetry. Numerical issues related to inversion matters as well as a discussion of uncertainties are considered in Section IV. Finally, REBEX-7 results are given in the last section.

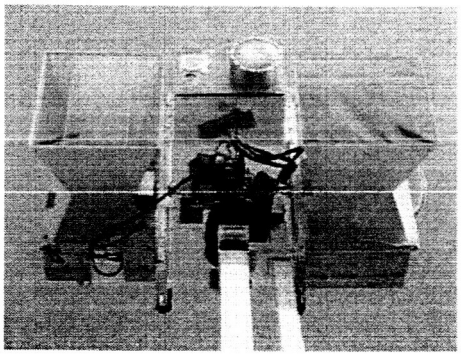

Fig. 1. ACMR mounted on the boom of the Truck Mounted Radiometer System during REBEX-7.

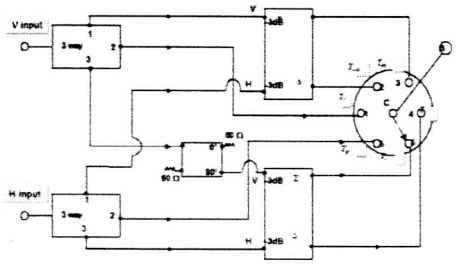

Fig. 2. Polarimetric combining circuit

II. FORWARD MODEL DESCRIPTION

A. Sensor description

The GSFC Airborne C band Microwave Radiometer (ACMR) was originally built as a dual-polarized (horizontal and vertical) radiometer centered at 6.8 GHz, with a 200 MHz bandpass, see 1 It features an analog additive circuitry to generate the $\pm 45°$ linear right hand and left hand circular polarizations. The sensor can be decomposed into four stages: (1) the antenna, followed by an orthomode transducer, (2) the remote receiver module (RRM) including calibration switches and low-noise amplification and filtering, (3) the polarimetric combining circuit (PCC) featuring a six-position electromechanical switch as illustrated in 2, and (4) the local receiver module (LRM), a gain chain with a square law detector diode. The LRM output is digitized by an analog/digital converter (ADC) and results are stored in a computer. This ADC subsystem is not examined in this paper. We note that the link between the detector and the computer is stable.

B. Forward model of blockwise calibration

1) Blockwise calibration concept: As described above, the ACMR architecture can be partitioned in several functional subsystems. Theoretically, if each subsystem is extensively measured and the estimated parameters are imported into an overcall transfer function describing the cascade architecture, a calibration may be obtained from a forward model based on actual system characteristics, as opposed to a classic end-to-end calibration based upon a standard target.

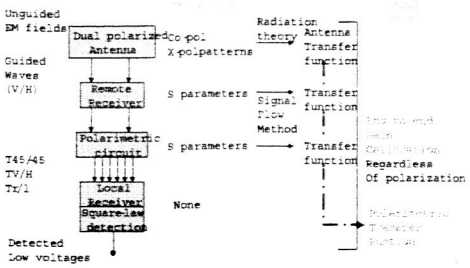

Fig. 3. Overall calibration approach

2) Choice of terminology: The input to the instrument can be formulated as brightness temperatures, or as electromagnetic fields. The instrument output consists of six voltages corresponding to the six detected polarizations. Each subsystem has a specific role in transforming the incoming wave, and special attention was given to the transfer function formulation in order to minimize numerical inversion noise and problems inherent to overdetermined matrices as later mentioned in section IV.

Let us consider a quasi-monochromatic wave incident on the antenna. A transition occurs through the antenna, transforming an unguided wave into a voltage at the V and H ports. We define an antenna transfer function transforming an unguided wave into voltages at the antenna ports, and transfer functions describing the Remote Receiver Module and Polarimetric Circuit behaviors. These three quantities can be derived from laboratory measurements that yield, respectively, antenna patterns, S-parameters for the RRM and S-parameters for the Polarimetric Circuit.

Since the PCC has a single output describing the amplitude of the combined signal for left, right, $+45°$ and $-45°$ polarization, and of the modified vertical and horizontal polarization, there are no phase imbalance or magnitude imbalance issues in any downstream elements of the instrument—i.e., the downstream configuration is equivalent to that of a single receiver. Only the gain, receiver self noise and input mismatch of the combined { LRM + ADC } are needed. These latter parameters are included in the end to end characterization of the ACMR, as we read directly the digitized detected amplified low voltage on the computer interface screen. The authors assumed that delays and attenuation of the signal were independent of the polarization. Using this approach, as shown in 3, we can derive a polarimetric transfer function as a combination of the signals' behaviors through the entire system, and therefore an end-to-end calibration for each polarization, assumed that the gain and the noise equivalent brightness temperature T_{rec} of the { LRM + ADC } combination is polarization-independent. The calibration of these latter two subsystems was obtained via a classic calibration as described in [8].

3) Forward model derivation: First, we considered the system { antenna+OMT+ two orthogonal polarizations in free space } as a four-port network [16]. However, this approach seems uncertain when we deal with unguided waves at the input. Therefore, we instead chose to use fundamental definitions from antenna radiation theory in order to link the input unguided fields to the output voltages at the OMT ports [17]. Suppose a dipole is fed by a 1A current, the field at a general receiving antenna is:

$$\begin{cases} E^i_\theta = \frac{jZ_o}{2\lambda r} e^{-jkr} L_{\theta'} \\ E^i_{\phi'} = \frac{jZ_o}{2\lambda r} e^{-jkr} L_{\phi'} \end{cases} \quad (2)$$

which can be rewritten as:

$$\vec{E}^i = \frac{jZ_o}{2\lambda r} e^{-jkr} \vec{L} \quad (3)$$

where $\vec{L}$ is the vector length of the dipole.
By reciprocity, the voltage output at the receiving antenna is:

$$\begin{aligned} V &= \frac{jZ_o}{2\lambda r} e^{-jkr} \vec{L}.\vec{h} \\ &= \vec{E}^i.\vec{h}(\theta,\phi) \end{aligned} \quad (4)$$

Where $\vec{E}^i$ is the impinging field on the antenna, and $\vec{h}(\theta,\phi)$ the effective length of the receiving antenna, equivalent to the pattern of that antenna in either receiving or transmitting mode. This effective length is the same as in the well known expression of the transmitted field of a general antenna:

$$\vec{E}^t = \frac{jZ_o}{2\lambda r} e^{-jkr} \vec{h}(\theta,\phi) \quad (5)$$

Hence, for any scene emitting a field $\vec{E}^i = \vec{E}^i_\theta \hat{u}_\theta + \vec{E}^i_\phi \hat{u}_\phi$, we can derive the relation between the voltage output of any antenna with the impinging electromagnetic field. For any scene emitting a field decomposed along the elevation and azimuth directions, the expected voltage outputs of the antenna are, respectively, for the V port and the H port:

$$\begin{cases} V_V = \int\int_{\Omega_p} (h^V_\theta E^i_\theta + h^V_\phi E^i_\phi) d\Omega \\ V_H = \int\int_{\Omega_p} (h^H_\theta E^i_\theta + h^H_\phi E^i_\phi) d\Omega \end{cases} \quad (6)$$

with:

- $h^V_\theta(\theta,\phi)$ corresponds to the ACMR pattern when the antenna is transmitting a vertically polarized wave and the Standard Feed Horn is receiving via its V port,
- $h^V_\phi(\theta,\phi)$ corresponds to the ACMR pattern when the antenna is transmitting a vertically polarized wave and the Standard Feed Horn is receiving via its H port,
- $h^H_\theta(\theta,\phi)$ corresponds to the ACMR pattern when the antenna is transmitting an horizontally polarized wave and the Standard Feed Horn is receiving via its V port,
- and $h^H_\phi(\theta,\phi)$ corresponds to the ACMR pattern when the antenna is transmitting an horizontally polarized wave and the Standard Feed Horn is receiving via its H port.

(6) accounts for the antenna non-idealities: phase delay at the antenna ports, mode leakage inside of the antenna, and gain imbalance between the two ports. In (6), we can see that imperfect polarization isolation is also considered.

First, as a first order approximation supported by measurement results described in section III, we will treat the observed scene as homogeneous, and the antenna sidelobe and backlobe contributions as negligible compared to the main lobe one of the antenna, due to the high main beam efficiency feature of the antenna. Moreover, for the purposes of REBEX-7, the

actual cornfield target is large and homogeneous enough for the approximation error to be negligible. (2) can be simplified using boresight values, yielding the following antenna transfer function:

$$\begin{cases} V_V = h_\theta^V E_\theta^i + h_\phi^V E_\phi^i) d\Omega \\ V_H = h_\theta^H E_\theta^i + h_\phi^H E_\phi^i) d\Omega \end{cases} \quad (7)$$

Second, let us consider the transfer functions associated with the RRM and PC following the antenna. We are interested in deriving the transfer function of cascaded networks from vector network analyzer(VNA) measurements. We choose the following notation: a_i and b_i are the incoming and outcoming power waves as in classic microwave network theory. For the four port network RRM, the input V port, input H port, output V port and output H port are respectively designated ports 1, 2, 3 and 4. Concerning the PCC, for each port excitation, and each switch position, a two-port network model is adopted. Through superposition, $[S_a]$, $[S_b]$, $[S_c]$, $[S_d]$, $[S_e]$, and $[S_f]$ are the scattering matrices for a vertical excitation and for the switch positioned at port 1, 2, 3, 4, 5 and 6, respectively. $[S_A]$, $[S_B]$, $[S_C]$, $[S_D]$, $[S_E]$, and $[S_F]$ correspond to the same switch positions for a horizontal excitation. According to the laboratory experimental results shown in section III, three levels of approximation can be adopted depending on the desired level of calibration accuracy. We can derive for each model, and each separate excitation port the resulting transfer function via signal flow graphs of the combined RRM and PCC. This symbolic approach, because of its analytical form, has the advantage of providing insight about the strengths and weaknesses of the instrument and therefore can serve as a simulator tool for future instrument designs. The second order approximation appears to be a good trade-off between complexity and accuracy for the ACMR case. Using superposition, the output of the PCC is the combination of the vertical and horizontal excitations at the input ports of the RRM:

$$b_3'' = \frac{s_{12}^a s_{31} a_1'}{1 - \Gamma_l s_{22}^a} + \frac{s_{21}^A (s_{41} a_1' + s_{42} a_2')}{1 - \Gamma_l s_{22}^A} \quad (8)$$

Inserting previous results into (8), we can write that:

$$b_3'' = A_3 E_V + B_3 E_H \quad (9)$$

Let us use complex expressions:

$$\begin{cases} A_3 = |A_3| e^{j\alpha_3} \\ B_3 = |B_3| e^{j\beta_3} \end{cases} \quad (10)$$

Also, let us use the decomposition of the fields as a combination of their magnitudes and frequency variations:

$$\begin{cases} E_V = E_v \cos(\omega t) \\ E_H = E_h \cos(\omega t - \delta) \end{cases} \quad (11)$$

Suppose the signal is being amplified by a gain G_{23}, then square law detected, and the user has access to an average of that number, hence:

$$\langle v_{out_3} \rangle = \langle |G_{23} b_3''|^2 \rangle \quad (12)$$

that is:

$$\langle v_{out_3} \rangle = \langle |G_{23}|^2 \{ |A_3|^2 |E_V|^2 + |B_3|^2 |E_H|^2 + 2\Re e(|A_3| |E_V| |B_3| |E_H| e^{j(\alpha_3 - \beta_3 + \delta)} \} \rangle \quad (13)$$

G_{23}, A_3, and B_3 are time independent, because they describe parts of the system that are thermally stabilized. Using linearity of the time averaging operator, and letting $C = \lambda^2/(k_B \eta)$, we can derive the expression of the output voltage for a noise free system:

$$\langle v_{out_3} \rangle = \frac{|G_{23}|^2}{C} \{ |A_3|^2 T_V + |B_3|^2 T_H + |A_3| |B_3| (\cos(\alpha_3 - \beta_3) T_3 - \sin(\alpha_3 - \beta_3) T_4) \} \quad (14)$$

The real system is equivalent to the noise free system described above, receiving the emission from the scene as well as the noise from the receiver itself. The equivalent receiver noise temperature translates into offsets that are added to each channel. The overall description of ACMR linking the output voltages to the modified Stokes vector of the scene under observation is:

$$\begin{pmatrix} \langle V_{out_3} \rangle \\ \vdots \\ \langle V_{out_8} \rangle \end{pmatrix} = \frac{1}{C} \begin{pmatrix} |G_{23}|^2 \\ \vdots \\ |G_{28}|^2 \end{pmatrix} \circ \begin{pmatrix} |A_3|^2 & |B_3|^2 \\ \vdots & \vdots \\ |A_8|^2 & |B_8|^2 \end{pmatrix} \begin{pmatrix} |A_3| |B_3| \cos(\alpha_3 - \beta_3) & -|A_3| |B_3| \sin(\alpha_3 - \beta_3) \\ \vdots & \vdots \\ |A_8| |B_8| \cos(\alpha_8 - \beta_8) & -|A_8| |B_8| \sin(\alpha_8 - \beta_8) \end{pmatrix} \begin{pmatrix} T_V \\ T_H \\ T_3 \\ T_4 \end{pmatrix} + \begin{pmatrix} offset_3 \\ \vdots \\ offset_8 \end{pmatrix} \quad (15)$$

where $\circ$ denotes a row by row multiplication. We will refer to this closed form expression as the polarimetric transfer function, which is similar in concept to the Jones matrix [18]. Most of the parameters in 15are known via the subsystem characterization. Two sets of parameters remain to be determined. The gains $G_{2i,i=3\ldots8}$ and the offsets $offset_{i,i=3..8}$ introduced by the receiver internal noise. By using a traditional end-to-end calibration with any un-polarized target at a known temperature, and by doing a term-by-term identification, the authors determined the last unknown parameters. This explicit determination of unknowns is valuable at this point, otherwise the system may be over-determined.

III. Experimental characterization

A. Critical antenna measurement for polarimeters

The radiative properties of an antenna are fully characterized by its radiation pattern, radiation efficiency, and polarization state. Conventional antenna measurements usually include E- and H-plane, cross and co-polarization patterns. For polarimetric radiometry, knowledge of phase imbalances and polarization purity is critical for later corrections.

1) Antenna measurement set up and protocol: The dual linearly polarized ACMR antenna is a C band circular corrugated horn antenna with a plano-convex lens over the horn aperture combined with the associated orthomode transducer (OMT). The antenna was designed and built by Microwave Engineering Corporation, North Andover, Massachusetts. It

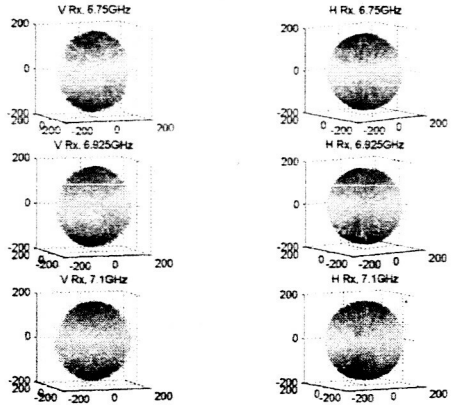

Fig. 4. Differential phase between the antenna vertical and horizontal ports. The antenna is looking in the upward vertical direction. The observer is situated in any position in space and sees the differential phase between the antenna ports as given by the length of the radius. A perfect antenna would yield a perfect sphere of radius 180°.

is centered at 6.925GHz, and features a HPBW of 12° and measured ohmic efficiency of 96% .

Definitions used for co-polarization and cross-polarization conform to Ludwig's third definition [19]. The test configuration is a transmit-receive system consisting of an oscillator and the test ACMR antenna as the transmitting antenna at the end of GSFC's tapered range anechoic chamber, rotating its head around its boresight (0 to 180°, in 2° increments), and rotating in azimuth around the test stand axis (-180 to 180°, in 1° increments). When set up for measurements, the ACMR antenna could only transmit either vertical or only horizontal polarization. The receive antenna, a Standard Feed Horn antenna, could receive both vertical and horizontal polarizations at the same time, and was connected to a phase coherent receiver. The two antennas are separated by a distance sufficient to insure that each antenna is in the far field of the other. Data was obtained for vertical and horizontal excitations separately and for three frequencies: 6.75GHz, 6.925GHz and 7.1GHz.

2) Results: There is a differential phase introduced by the ACMR antenna between V and H output ports for the vertical or horizontal input polarization at several frequencies over the radiometer passband. If the antenna were perfect, the differential phase would be 180°, since the boresight-axis offset distance between the output ports is half a wavelength. 4 illustrates the antenna phase non-ideality. The plot is equivalent to having the antenna positioned in coordinates (0, 0, 0), and having the antenna under test simultaneously transmitting V and H polarizations in phase. "V Rx" means the observers look at the feed horn V port in the co-pol and cross-pol plane [19]. Hence, the read phase difference is introduced by the ACMR as a perfect sphere of radius 180° and does not appear on the plots.

Additionally, the input VSWR at the OMT ports was 15dB and the VSWR variability as a function of distance to black body calibration target was negligible. The isolation between the ports was greater than 50dB.

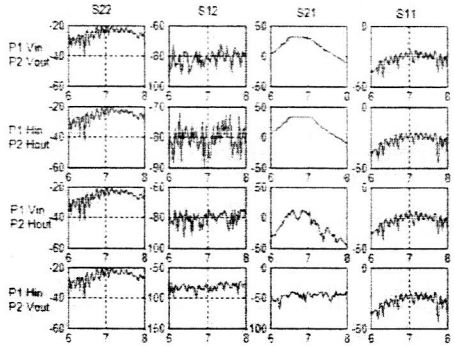

Fig. 5. Magnitude of RRM cross talk between the vertical and the horizontal channels. For measurement purposes, the RRM was treated as a two port network. The four rows correspond to the four combinations of input and output ports. Port 1 and Port 2 are, respectively, the output and input port of the RRM. The columns correspond to the four measured scattering coeffi cients. The horizontal axis represent the frequency component.

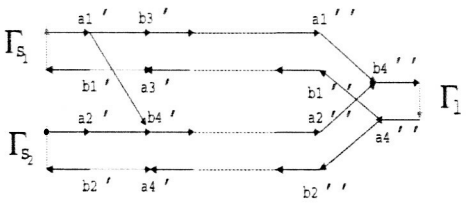

Fig. 6. Equivalent signal flow chart for the combined RRM and PCC system. Reflections looking into the ports are represented by Γ. Note the path a1'–b4' represents the signal leakage mentioned in the text.

B. Vector Network Analyzer measurement of RRM and PCC

The RRM was tested with a HP8510 VNA between 6 and 8 GHz in the following way. First, we considered the two port network consisting of the input V port and the output V port, second the two port network consisting of the input H port and the output H port. We also checked the isolation between the two input ports, and between the two output ports. Finally, we measured the forward cross talk between the two channels. We note there is a non-negligible signal leakage (tens of dB over the passband) from the vertical channel into the horizontal channel occurring in the RRM, see5. The blockwise calibration approach not only handles this, but identifies the RRM as the culprit. On the signal level, the signal flow graph used to describe the RRM+PCC subsystem is presented in 6.

C. Local Receiver Module/ADC

The only measurement performed on the LRM was the measurement of the input VSWR, denoted Γ_l in the previous section. During the measurements, the RF port is being square law detected therefore not terminated, and the first component seen by the VNA is an isolator. These facts account for the input VSWR of 0.35.

D. End to end system characterization

Since the signal goes through different paths depending on the switch position, the authors performed an end to end

calibration of the radiometer for each one of the six switch positions. The antenna viewed an un-polarized absorber target at ambient temperature ($27°C$) and at liquid nitrogen temperature (77K). The output voltages corresponding to the six different switch positions and 30 second integration time were recorded. To ensure stable target temperatures, only integrations having a standard deviation on the order of 10^{-4} were used. Using linear interpolation, we obtain for each switch position, the equivalent independent radiometer gains and receiver noise temperatures. On average, the equivalent noise temperature is 266.5K for a standard deviation of 4.3K, e.g. 1.6%. This is consistent with the low-noise amplifier (that is upstream of the PCC and its switch) dominating the noise figure. Therefore, as a first-order approximation, we can consider that the equivalent noise temperature is the same for all switch positions.

IV. NUMERICAL ISSUES

A. Error analysis

We showed how the polarimeter forward model describes the actual operation of the polarimeter. Because the forward model is based on actual laboratory measurements, any uncertainty on measurement parameters will affect the final result, regardless of the operation mode of the polarimeter. For instance, if the integration time of the ACMR is modified, the radiometer sensitivity will change, but uncertainties coming from the inversion of the laboratory-based transfer function will still remain the same.

Let us determine the errors associated with the analytical approach. [21] recommends that all uncertainties be expressed in a standardized way. According to classical error analysis definitions [20]: (15) is the measurement equation, the state vector to be retrieved is the four modified Stokes parameters. To gain a better understanding of the uncertainties in the estimation of the state vector, we can categorize the errors according to their origin:

- Jones' matrix is based on laboratory measurements that are inherently subject to experimental errors. These *forward model parameter errors* are given by the measuring instrument manufacturers and the measurement set up.
- *Retrieval error*, e.g. error in the retrieval due to the total output voltage measurement error, corresponds for instance to a rounding error in the case of ACMR.
- Since the transfer funtion is based on the true physics of the ACMR system, there is no *forward modelling error*. In particular, we check that the *bias*, e.g. error that would result from a simulated retrieval using a simulated error-free measurement of the a priori state computed with the forward model is zero indeed.

Concerning the characterization of the observing system, there is no sensitivity of the retrieval to the true state, since the system had been specifically designed for geophysical brightness temperature input ranges.

Once we have define the different sources of uncertainties, we can also classify them in two categories: random or systematic. An example of systematic error is the phase imbalance between ACMR channels. The total uncertainty of the estimated Stokes parameters can be obtained with the law of propagation uncertainty. This law consists in combining the individual standard uncertainties arising from random and systematic error evaluations.

Applying the procedure shows that at worst the analytical calibration approach applied to the ACMR yields an uncertainty of 0.2K for the retrieval of the estimated values of (T_v and (T_h. Concerning the retrieval of the third and fourth modified Stokes parameters, applying a calibration based on laboratory measurements guarantees an uncertainty of less than 2.4K. These errors are relatively small due to the quality of modern test equipment (for example, our VNA had a phase sensitivity of $0.02deg$). We can expect these uncertainties to decrease as testing equipement performances improve.

B. Potential of transfer function as an instrument simulator

The polarimetric transfer function describing the actual operation of the intrument constitutes a valuable engineering tool. First, this function can serve as a performance assessment tool at the overall level. Inspection of the numerical components of the transfer matrix shows for instance:

- the vertical output voltage is well protected from any leakages. Contributions to this channel from other components are down to -30dB.
- the overall system design is acceptable. Although the transfer matrix yields an overdetermined system, the system is easily inversible as shown by its rank of 4 and its conditioning number of 5, which is relatively close to 1. The use of standard commercial software inversion algorithm proved to be enough without the need of regularization tools.

Additionally, the polarimetric transfer function 15 can be used as a simulator for future instruments that would be based on the original ACMR design. One possible future investigation would be to simulate the correction of the leakage of the vertical-polarized signal into the horizontal channel, or the correction of the antenna phase imbalances, then observe the consequences of the conditionning of the matrix, and therefore see if these corrections permit a smoother inversion, and consequently more reliable estimates of the modified Stokes parameters. From the opposite viewpoint, the simulator can also be used as a worst-case scenario evaluation tool by answering questions such as: how much gain or phase imbalances make the system unusable? Which functional block is the most critical in terms of polarization isolation? Answers to these questions would provide specifications for analog non-idealities, and guarantee retrievable data if these minimum requirements are met.

V. APPLICATION TO REBEX-7

A. Background and measurements

Wet soils have large permittivities and surface fields can display large special variations. Thermal emissions of soils with rough surfaces depend on the surface roughness, soil moisture, soil type and physical temperature. However , the presence of a canopy complicates the retrieval of moisture in the underlying soil because the canopy scatters and contains moisture of its

Fig. 7. Truck Mounted Radiometer system in corn field during REBEX-7

Fig. 8. Row configuration of cornfield during experiment. The rows are oriented along the North-South direction.

own. Then, the microwave emission from the surface depends on the soil moisture, surface temperature, surface roughness and attenuation through the vegetation canopy overlying the surface. In order to increase the understanding of the sensitivity of microwave emission to soil moisture and vegetation biomass, the Radiobrightness and Energy Balance Experiment 7 was held in Michigan in October 2000 over a cornfield, see 7 and 8. The main objective was the monitoring of soil and vegetation processes using multisensors and multitemporal observations. Other sensors include radiometers at L band, 19GHz and 37GHz, as well as a standard micrometeorological station. End to end calibration used the sky and a box absorber at ambient temperature. Ground samples of soil and vegetation were also collected.

B. Results

(15) was used to retrieve the full modified Stokes parameters over a cornfield. Previous work show that at L band frequencies, both polarizations of brightness are isotropic during most of the growing season of corn [22]. As the canopy becomes

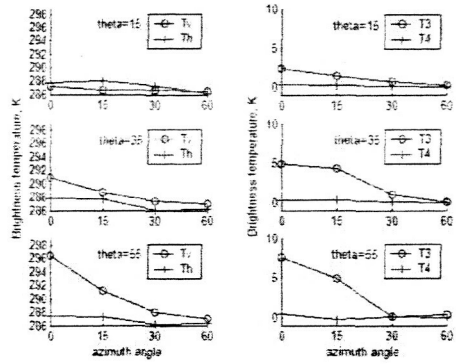

Fig. 9. Senescent polarimetric signal at C band on October, 10, 2000 at noon. The left column displays the vertical and horizontal brightness temperatures. The corresponding third and fourth Stokes parameters are displayed on the right column. Brightness temperature variations are shown as a function of the azimuth angle ϕ along the horizontal axis and as function on the incidence angle θ along the vertical direction.

senescent, the brightness evolves as a strong function of row direction [23]. At senescence, the leaves loose their water, and are transparent at L band. A preliminary interpretation of the data shows that the brightness temperature is a function of the row direction at C band too, as illustrated in 9. Near nadir, the vertical and horizontal brightness temperatures are almost equal, and the third and fourth Stokes parameters close to zero, therefore the cornfield behaves like a back body from the standpoint of the polarimeter. At higher incidence angles, the polarimeter senses the structure of the cornfield, and the vertical and horizontal polarized signals differ. Accordingly, the third and fourth modified Stokes parameters take non-zero values. More in-depth further studies should take into account the vegetation temperature variation, and other available meteorological data.

VI. Conclusion

A robust blockwise calibration based on well-controlled laboratory experimental characterization was used to calibrate the ACMR. The authors partitioned the system into functional blocks, that could be easily characterized. The estimated parameters were exported into a polarimetric transfer function describing the instrument,including hardware imperfections. Uncertainties in calibration parameter values and therefore uncertainties of the final calibration were due mainly to noise in the measurement, yielding 0.2 K uncertainty for the V and H polarizations and 2.4 K uncertainty for the 3rd and 4th modified Stokes parameters. As testing equipement performance improves, uncertainties inherent to the analytical calibration are expected to decrease and be less that 2K for the third and fourth parameters. Emphasis was given concerning one of the most useful characteristics of the approach, that quantitative parameters can be obtained from the polarimetric transfer function, when it is used as a simulator. Based on this calibration, the first polarimetric brightness observations at C band over senescent corn are presented. A polarimetric signal that depends on the azimuth angle appears to exist. A combined analysis with L band data should allow the

separation of soil and vegetation contribution in the brightness temperature signal. These results are important to better understand the effects of complex canopies on the microwave thermal emission of soils.

ACKNOWLEDGMENT

The authors wish to thank S. Seufert, R. Rincon, T. Dod, K. Hersey and J. Piepmeier at NASA/GSFC and A. Imig. They are also grateful for T. England, C. Ruf, R. Deroo, E. Choinière, and B. Hornbuckle's comments at the University of Michigan.

REFERENCES

[1] A. K, Betts, and P. Viterbo,"The Land-surface atmosphere interaction: A review based on observational and global modeling perspectives," J. Geophys. Res., vol.101, pp.7209-7225, 1996

[2] J. P. Peixoto, and A. H. Oort, Physics of climate, New York: American institute of Physics, 1992.

[3] T. Schmugge, P. Gloersen, T. Wilheit, and F. Geiger, "Remote sensing of soil moisture with microwave radiometers," J. Geophys. Res., vol.79, no.2, pp.317-323, Jan.1974

[4] Y. A. Liou, J. F. Galantowicz, and A. W. England, "A land surface process/radiobrightness model with coupled heat and moisture transport for prairie grassland," IEEE Trans. Geosci. Remote Sensing, vol. 37, no.4, pp.1848-1859, July 1999.

[5] L. Tsang, "Polarimetric passive microwave remote sensing of random discrete scatterers and rough surfaces," J. Electromagnetic waves and applications, vol.5, no.1, pp.41-57, 1991

[6] J. R. Piepmeier and A. J. Gasiewski, "High-resolution passive polarimetric microwave mapping of ocean surface wind vector fields," IEEE Trans. Geosci. Remote Sensing, vol. 39, no. 3, pp. 606-622, Mar. 2001a.

[7] S. V. Nghiem, M. E. Veysoglu, J. A. Kong, and R. T. Shin, "Polarimetric passive remote sensing of a periodic soil surface: microwave measurement and analysis," J. Electromagnetic waves and applications, vol.5, no.9, pp. 997-1005, 1991

[8] F. T. Ulaby, R. K. Moore, and A. K. Fung, Microwave remote sensing, active and passive. Norwood, MA: Artech House, 1981, vol.1.

[9] N. Skou, B. Laursen, and S. Sbjrg, "Polarimetric radiometer configurations: Potential accuracy and sensitivity," IEEE Trans. Geosci. Remote Sensing, vol. 37, no. 5, pp. 2165-2171, Sept. 1999.

[10] A. B. Tanner, and C. T. Swift, "Calibration of a synthetic aperture radiometer, " IEEE Trans. Geosci. Remote Sensing, vol. 31, pp.257-267, Jan. 1993

[11] J. Lahtinen, PhD dissertation, Helsinki University of Technology, 2003

[12] E. J. Kim, B. Davis, J. R. Piepmeier, "A common calibration source framework for fully polarimetric and interferometric radiometers," First International Microwave Radiometer Calibration Workshop, October 3031, 2000, College Park, MD

[13] J. R. Piepmeier, E. J. Kim, "Calibration of passive microwave hybrid coupler-based polarimeters" Geoscience and Remote Sensing Symposium, 2003. IGARSS '03. Proceedings. 2003 IEEE International, Volume: 2 , 21-25 July 2003 Pages:1244 - 1246 vol.2

[14] C. S. Ruf," Detection of calibration drifts in spaceborne microwave radiometers using a vicarious cold reference," IEEE Trans. Geosci. Remote Sensing, vol. 38 , no. 1 , pp:44 - 52, Jan. 2000

[15] C. Ruf, and J. Li, "A correlated noise calibration standard (CNCS) for interferometric, polarimetric, and autocorrelation microwave radiometers," IEEE Trans. Geosci. Remote Sensing, vol. 41, no.10, October 2003

[16] W. L. Stutzman, Polarization in electromagnetic systems, Artech house, 1993

[17] H. Mott, Antennas for radar and communications, a polarimetric approach. Wiley series microwave and optical engineering, 1992.

[18] J. P. Hamaker et al, "Understanding radio polarimetry (I)," Astronomy and astrophysics supplement series. 117, 137-147 (1996)

[19] A. C. Ludwig, "The definition of cross-polarization," IEEE Trans. Antennas and Propagation, vol. 21, pp.116-119, January 1973

[20] C. D. Rodgers, Inverse methods for atmospheric sounding: theory and practice, Series on Atmospheric, oceanic and planetary physics, vol.2, World scientific", 2000

[21] ISO, "Guide to the expression of uncertainty in measurement," Int. Standards Org. , Geneva, Switzerland, 1995

[22] S. S. Sobjaerg, N. Skou,"Polarimetric signatures from a crop covered land surface measured by an L-band polarimetric radiometer," Geoscience and Remote Sensing Symposium, 2003. IGARSS '03. Proceedings. 2003 IEEE International, vol. 4, pp.2626 - 2628, 21-25 July 2003.

[23] B. K. Hornbuckle, A. W. England, R. D. DeRoo et al, "Vegetation canopy anisotropy at 1.4GHz," IEEE Trans. Geosci. Remote Sensing, vol. 41, pp.2211-2223, Oct. 2003

Hanh Pham received the engineer diploma from the Ecole Supérieure D'Electricité (SUPELEC), Gif-sur-Yvette, France, in 2002, the M.S.E degree in electrical engineering (electromagnetics and signal processing) from the University of Michigan, Ann Arbor, in 2003. She is currently pursuing the Ph.D. degree in electrical engineering at the University of Michigan. She was with NASA Goddard Space Flight Center, Greenbelt, MD, as a summer intern in 2002 and 2003. Her research interests include radiometer system calibration, and noise signal processing.

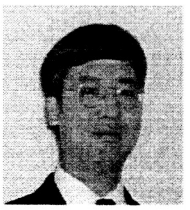

Edward Kim (S'90, M'99) received the SB, SM, and Engineer's degrees in Electrical Engineering from the Massachusetts Institute of Technology. He completed a joint PhD with the Departments of Electrical Engineering and Atmospheric Sciences at the University of Michigan in 1998. Since 1992, he has been involved in remote sensing field experiments related to the cryosphere, land, atmosphere, and oceans. In 1997, he was selected for a National Research Council Research Associateship, and in 1998, he was awarded 2nd prize in the International Geoscience and Remote Sensing Symposium student paper competition. Dr. Kim has been at NASA's Goddard Space Flight Center since 1999, in the Microwave Sensors Branch, developing and applying Earth remote sensing techniques. His interests include the modeling of snow, ice, soil, and vegetation; radiative transfer theory; and microwave and optical instrumentation. He is the GSFC Project Scientist for the Cold Land Processes Pathfinder mission concept. Dr. Kim is a member of the IEEE and the American Geophysical Union.